Bioinspiration & Biomimetics

PAPER

An experimental study on the mechanics and control of SMA-actuated bioinspired needle

RECEIVED
2 June 2023

REVISED
22 August 2023

ACCEPTED FOR PUBLICATION
19 September 2023

PUBLISHED
28 September 2023

Sharad Raj Acharya and Parsaoran Hutapea*

Department of Mechanical Engineering, Temple University, Philadelphia, PA, United States of America
* Author to whom any correspondence should be addressed.

E-mail: hutapea@temple.edu

Keywords: bioinspired needle, friction, insertion force, tip deflection, needle tracking control

Abstract

Active needles demonstrate improved accuracy and tip deflection compared to their passive needle counterparts, a crucial advantage in percutaneous procedures. However, the ability of these needles to effectively navigate through tissues is governed by needle-tissue interaction, which depends on the tip shape, the cannula surface geometry, and the needle insertion method. In this research, we evaluated the effect of cannula surface modifications and the application of a vibrational insertion technique on the performance of shape memory alloy (SMA)-actuated active needles. These features were inspired by the mosquito proboscis' unique design and skin-piercing technique that decreased the needle tissue interaction force, thus enhancing tip deflection and steering accuracy. The bioinspired features, i.e., mosquito-inspired cannula design and vibrational insertion method, in an active needle reduced the insertion force by 26.24% and increased the tip deflection by 37.11% in prostate-mimicking gel. In addition, trajectory tracking error was reduced by 48%, and control effort was reduced by 23.25%, pointing towards improved needle placement accuracy. The research highlights the promising potential of bioinspired SMA-actuated active needles. Better tracking control and increased tip deflection are anticipated, potentially leading to improved patient outcomes and minimized risk of complications during percutaneous procedures.

1. Introduction

Percutaneous needles play a vital role in various medical procedures such as biopsy and brachytherapy, where they must reach precise locations within tissues such as the liver, prostate, kidney, and brain for sampling or cancer treatment. The effectiveness of these minimally invasive procedures depends on the needles' ability to accurately reach the target location inside the tissues to collect samples or treat cancer. Often, surgeons want to avoid obstacles such as critical nerves and blood vessels and prefer large tip deflection to achieve a curved path of needle travel. Needle steering is defined by the mechanical interaction between the needle and the tissue. Many researchers have designed and studied innovations in surgical needles to reduce insertion force and tissue deformation [1, 2]. Conventionally used flexible needles with a bevel tip have limitations in tip deflection and steering toward the target. The tip deflection is small and depends on the needle tissue interaction. The nonlinearity and heterogeneity of tissues make the deflection of the passive needles unpredictable [3]. Active needles are designed to provide controlled deflection during tissue insertion [4–6]. However, these needles cannot fully compensate for unexpected bending and tissue deformation. The needle buckling is affected by tissue interaction forces [7], which have been positively correlated with tissue deformation [8] and tissue damage [9]. Reducing the tissue interaction forces in active needles would also reduce the needle buckling, tissue deformation, and tissue damage paving a path for improving the desirable large tip deflection and better steering accuracy.

The needle tissue interaction force, measured with insertion force at the needle base, involves pre-puncture tissue stiffness force and post-puncture cutting force at the needle tip and friction force along the needle shaft [10]. The post-puncture needle insertion force can be reduced by changing parameters such as needle geometry, insertion velocity, and insertion method (vibration and rotation) [1, 11]. The needle

geometry involves the tip and the shaft. The cutting force at the tip includes the plastic deformation from the act of cutting and the force resulting from tissue stiffness. Several studies have been conducted on modifying needle tip geometry to reduce the cutting forces [12–15]. A bevel tip needle has a smaller cutting force than a conical tip needle [15] but unlike a conical tip needle, it cannot travel in a straight path without rotating the needle about its axis. The friction force develops at the needle shaft after the needle punctures the tissue, increasing as the needle is driven deeper into the tissue [16]. It is the most significant contributor to the insertion force, especially for deep tissue insertions. The friction force per unit length of the needle increases as the insertion velocity increases, but the cutting force does not increase as much as the friction force [17].

Several methods have been adopted to reduce the friction force on the needle shaft during the tissue insertion process. Patel *et al* [18] used a method of composite coating on the needle shaft that functioned as a dry lubricant to reduce the friction force. Other researchers have studied the needle designs and insertion mechanisms inspired by the insect parts such as honeybee stinger [19, 20], mosquito proboscis [21–24], and wasp ovipositor [25]. Gidde *et al* [24] studied the effect of vibration and bioinspired design in the needles in reducing the insertion force and found a 50% reduction in polyvinyl chloride (PVC) gel and a 43% reduction in chicken breast. Experiments with mosquito-inspired design and vibrational insertion of passive needle prototype into PVC gel resulted in a 60% reduction in insertion force [23], a 48% reduction in tissue deformation [23], and a 27% reduction in tissue damage [9]. While the bioinspired features (needle surface geometry and vibrational insertion method) have been explored in passive needles for reduced friction, the potential benefits in active needles have not been studied.

The goal of this study was to investigate the changes in the needle-tissue interaction mechanics and deflection tracking control due to the addition of bioinspired features in an active steerable needle. The bioinspired features included the surface geometry of mosquito proboscis and the vibrational insertion method. The first hypothesis was that including these bioinspired features in an active needle would reduce the insertion force but increase the active tip deflection. The second hypothesis was that these features would reduce the deflection tracking error and control effort, thus improving the trajectory tracking control during insertion into a tissue. To test these hypotheses, the cannula of the shape memory alloy (SMA)-actuated active needle designed by Acharya and Hutapea [6] was modified to include a mosquito proboscis-inspired surface geometry. The SMA-actuated needle was used because it could actuate variable needle tip deflection that could be controlled during tissue insertion. Similarly, a piezoelectric vibration actuator was added to the base of the needle for the vibrational insertion method.

The outer surface of the cannula accommodated a maxilla structure- a jagged structure found in mosquito proboscis [26]. Gidde *et al* [23] scaled up the maxilla structure of mosquito proboscis for a 3 mm diameter 3D printed needle prototype. In this study, we used the scaled-up dimension of the maxilla structure applied by [23] into the cannula of the SMA-actuated needle. With the modified cannula, the outer diameter of the SMA-actuated needle prototype was 3.5 mm. A clinically relevant size would be 14 gauge (2.11 mm diameter) and smaller, but we could not manufacture the needle at this scale. However, Acharya and Hutapea [5, 6] have argued that their design of SMA-actuated needle could be reduced to a clinically applicable scale with the advancement in manufacturing technology, especially by reducing the thickness of the SMA attachment region in the needle. Past studies on bioinspired passive needle design with scaled-up diameter showed insertion force reduction, which was also seen in needles with clinically applicable diameters [11, 19]. We assumed similar changes would be seen in the bioinspired active needle mechanics and control when the needle diameter is scaled down. First, we aimed to evaluate if the bioinspired cannula design (maxilla structure in cannula surface) in the SMA-actuated needle reduced the insertion force and increased the tip deflection for the same amount of SMA actuation during the insertion into a tissue. Next, we needed to see if the vibrational insertion method reduced the insertion force and increased the needle tip deflection. Finally, we wanted to check if the bioinspired cannula design and the vibrational insertion method in the SMA-actuated needle reduced the deflection tracking error and control effort during tissue insertion. To the authors' knowledge, this is the first study exploring the benefits of bioinspired features (bioinspired cannula design and vibrational insertion method) on SMA-actuated active needles.

2. Materials and methods

The materials and methods used in this study are divided into five sections. The first section includes designing and fabricating a bioinspired cannula for the SMA-actuated active needle. The second section introduces the tissue-mimicking PVC gel used in this study and its fabrication. The method to evaluate needle friction during tissue insertion is described in the third section. The fourth section elaborates on the experimental approach to evaluate the change in insertion force and needle tip deflection during tissue gel insertion. The fifth and final section explains the deflection tracking control on tissue gel and the measurement of control parameters used to evaluate and compare the needles.

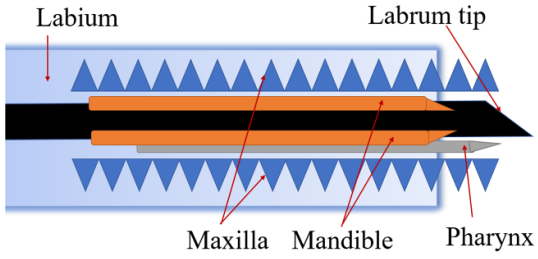

Figure 1. Schematic representation of mosquito proboscis showing five different components.

2.1. Design and fabrication of bioinspired cannula

The geometry of the cannula surface was inspired by the maxilla structure of the mosquito proboscis shown in the schematic figure 1. The components of a mosquito proboscis are labium, labrum, pharynx, mandibles, and maxilla [27, 28]. The maxilla structure of mosquito proboscis is about 20–40 μm in diameter and 1.5 mm to 2.5 mm in length [27]. The maxilla profile was transferred to the 2.60 mm diameter, 180 mm long polytetrafluoroethylene (PTFE) cannula tube of the SMA-actuated needle proposed by Acharya and Hutapea [6]. A stainless-steel stylet of 1.28 mm diameter was inserted inside the compliant PTFE cannula tube of 2.60 mm diameter. In the tip region of the stylet, a 40 mm long and 0.85 mm deep slot was created. In the slot, a 30.50 mm long, 0.20 mm diameter SMA wire actuator was attached to actuate the needle tip deflection upon heating the SMA wire with electric power (see figure 2(a)) [6]. The SMA wire, obtained from Dynalloy Inc. company in a trained condition, produced a maximum transformation strain (contraction) of 4.5% upon full actuation (heating to 100 °C). The 180 mm long SMA-actuated needle produced a tip deflection of 39 mm at 150 mm insertion depth into prostate-mimicking (PM) tissue gel [6]. The jagged-like structure of the maxilla was transferred to the PTFE cannula tube by creating a circular barb. The circular barbs were created by 3D printing the maxilla profile on a plane polymer sheet and then rolling it onto the surface of the PTFE tube. In this study, we anticipated that adding a 3D printed sheet would increase the stiffness of the needle and slightly reduce the tip deflection. However, the variations in cannula designs and insertion methods would produce significant differences in the magnitudes of tip deflection for the SMA-actuated needles.

The proposed dimensions of the maxilla for the cannula were chosen based on the dimension used by Gidde *et al* [23] on a mosquito-inspired passive needle. They performed a parameter study on 3 mm diameter scaled-up mosquito-inspired passive needles and found that the maxilla angle M_A and maxilla spacing M_S of the barbed structure were the only influential parameters that caused a significant change in the insertion force. They obtained the lowest insertion force for the needle design with maxilla parameters: $M_A = 170°$ and $M_S = 0.2$ mm, which was also applied in the cannula design in this study. Thus, the mosquito proboscis-inspired cannula with the surface geometry parameters optimized by Gidde *et al* [23] was designed, fabricated, and installed into the SMA-actuated active needle. Figure 2(a) shows the tip bending region of the active stylet, and figure 2(b) shows the active needle after inserting the stylet into a compliant PTFE tube [6, 29]. The maxilla surface profile was 3D printed with a Stratasys J35 printer using a polyjet rubberlike material called Elastico^{TM} (figure 2(c) shows the 3D design on the left and 3D printed sheet with maxilla surface profile on the right). The 3D printed flexible polymer sheet (180 mm long, 8 mm wide and 0.45 mm thick) was rolled on PTFE tube outer surface along its entire length. The polymer sheet was glued using gorilla glue while rolling on the PTFE tube. The glue application in the PTFE tube was made at the same locations for the regular and maxilla profile sheets to prevent an ununiform effect on the cannula stiffness. Figure 2(d) shows the SMA actuated needle with bioinspired and regular cannula design. The outer diameter of the needle prototype with the regular cannula and bioinspired cannula design was 3.5 mm. The 3D view of the SMA-actuated needle showing the components such as needle stylet, SMA wire, PTFE tube, 3D printed maxilla profile sheet forming a cannula, and position sensor attached to the bottom of the needle are shown in figure 2(e). To add the position sensor to the needle, a slot was created at the bottom of the cannula when rolling the 3D printed sheet on the PTFE tube. The addition of the position sensor (0.56 mm diameter) increased the effective diameter of the needle to 3.61 mm (as shown in figure 2(e)).

The active needles were tested using a robotic needle insertion setup, as shown in figure 3, which consisted of linear stage unislide to insert the needle into tissue phantom gel along the Z-direction. The SMA actuator was powered with pulse width modulated (PWM) power [6] to control the tip deflection along the XZ plane (horizontal plane). A piezoelectric actuator (Physik Instrumente, Auburn, MA) and a six-axis Force/Torque Transducer Nano17® (ATI Industrial Automation, Apex, NC) were installed at the needle base for applying longitudinal vibration and measuring the insertion force during the active needle insertion into PVC gel. Similarly, an electromagnetic (EM) position sensor (NDI, Canada) was used to measure the active needle tip deflection during tissue insertion.

2.2. Preparation of prostate mimicking (PM) gel

The SMA-actuated needles with two different cannulas were tested with constant actuation and deflection tracking control in PM tissue phantom gel (see figure 3). Ahn *et al* [30] reported that the mean elastic modulus of the prostate gland in the cancerous region

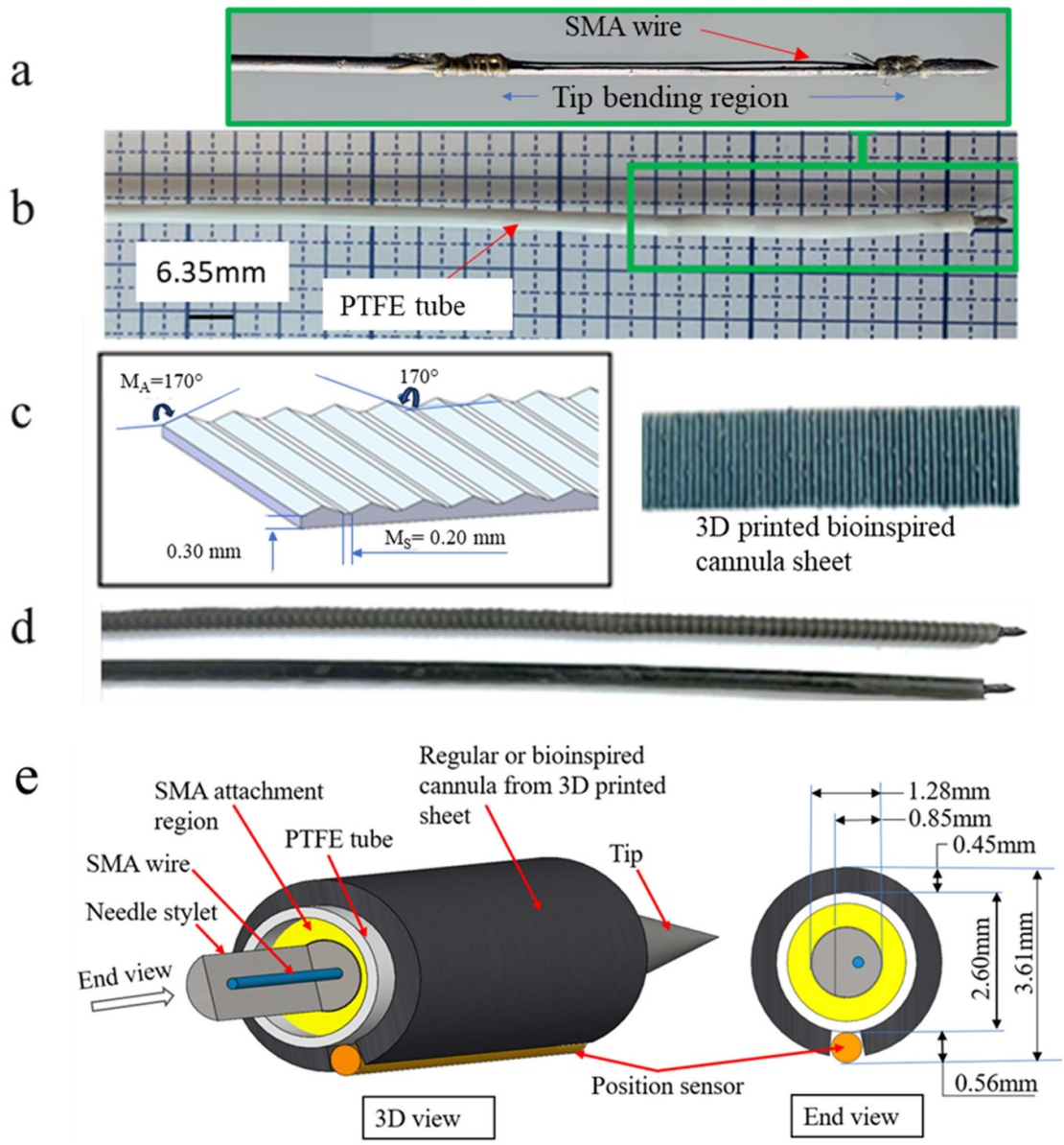

Figure 2. (a) Active needle stylet showing tip bending region with SMA wire actuator, (b) active needle after inserting the stylet into the compliant PTFE tube (outer diameter: 2.60 mm), [6] John Wiley & Sons. © 2023 John Wiley & Sons Ltd. (c) Solid model showing maxilla design parameters: maxilla angle M_A and maxilla spacing M_S (left) and 3D printed maxilla sheet (right), (d) Bioinspired cannula (top) and regular cannula (bottom) after rolling onto the surface of the PTFE tube, (e) 3D view (left) and end view (right) showing different components of SMA-actuated needle with modified cannula (3D printed polymer sheet rolled onto PTFE tube outer surface) and position sensor attachment [6].

was 24.1 ± 14.5 kPa, and in the noncancerous region was 17.0 ± 9.0 kPa. In this study, PVC tissue gel of elastic modulus 20 kPa were prepared to represent prostate glands. They were produced by mixing PVC polymer solution and diethyl hexyl adipate softener (M-F Manufacturing, Ft. Worth, TX) in a ratio of 60:40 according to the method described by Li *et al* [31]. The elastic modulus of the PVC gel was measured with the cylindrical sections of the gels (height (h) = 19 mm, diameter (d) = 40 mm) using a customized compression test setup, as shown in figure 4. The elastic modulus was calculated from the force–displacement data acquired from the tissue gel compression test performed for 10 mm compression at 2 mm s^{-1}. The elastic modulus of the PVC gel was obtained to be 21.00 ± 2.85 kPa.

2.3. Measurement of needle tissue interaction friction

The friction force on the needle shaft during tissue insertion is due to Coulomb friction and damping. Okamura *et al* [16] measured the needle-tissue interaction friction by performing a needle insertion-extraction test on a liver lobe with a sinusoidally changing velocity. The needle shaft interacted with the tissue without the tip touching the tissue, as shown in figure 5. They measured the axial force at the needle base to calculate the friction parameters such

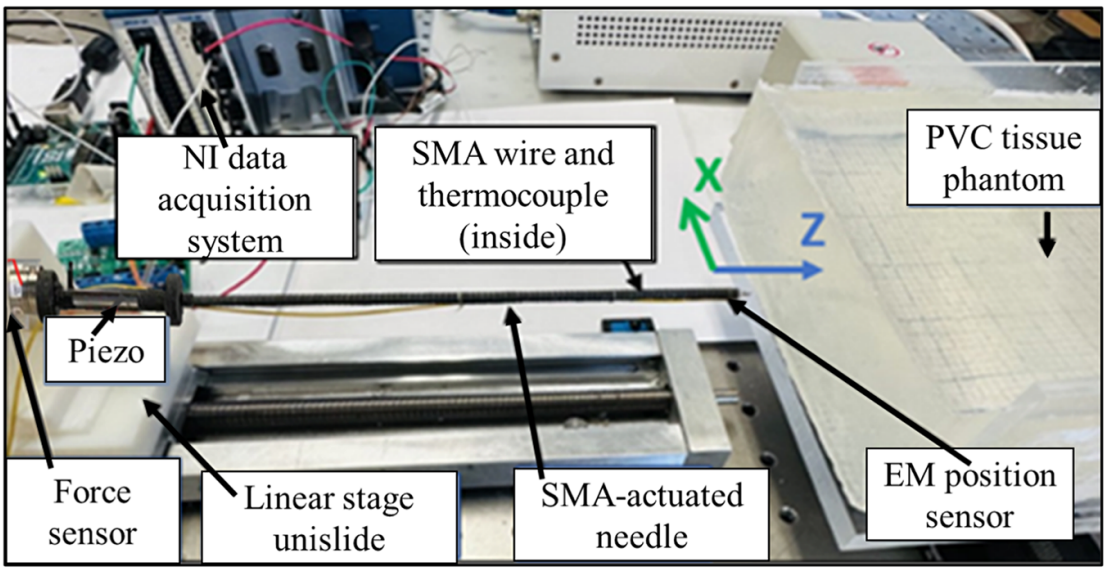

Figure 3. Robotic needle insertion setup for inserting and actuating deflection inside tissue phantom.

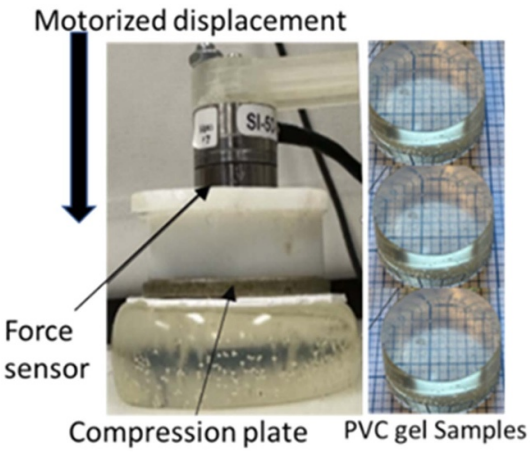

Figure 4. PVC gel uniaxial compression testing.

as Coulomb friction and damping coefficient. The friction calculation was motivated by the data analysis technique performed by Richard *et al* [32], which applied a least square regression to relate the sinusoidal velocity to the measured friction during the sliding of two surfaces.

The friction force model can be written as follows:

$$F_{\mathrm{f}}(h,\dot{z}) = \left\{ F_{\mathrm{C}}(h,\dot{z}), F_{\mathrm{v}}(h,\dot{z}) \right\} \quad 0.5\ \mathrm{mm\ s^{-1}} \leqslant \dot{z} \leqslant V_{\max} \tag{1}$$

where F_{f}, F_{C} and F_{v} are the total friction, Coulomb friction, and viscous forces, respectively. h and $\dot{z}$ are the width of the tissue and relative velocity between the needle and the tissue, respectively. $\dot{z}$ was assumed to be zero for the needle velocity below the magnitude of 0.5 mm $\mathrm{s^{-1}}$. We measured the friction force for a sinusoidal velocity of 4 mm $\mathrm{s^{-1}}$ amplitude. Equation (1) was simplified to estimate force parameters at non-zero velocities, as shown in equation (2),

$$F_{\mathrm{friction}} = \left[F_{\mathrm{CP}} sgn(V_{\mathrm{P}}) + b_{\mathrm{P}} V_{\mathrm{P}} + F_{\mathrm{CN}} sgn(V_{\mathrm{N}}) + b_{\mathrm{N}} V_{\mathrm{N}}\right] h \tag{2}$$

where $V_{\mathrm{P}}, b_{\mathrm{P}}, F_{\mathrm{CP}}$ are the positive (needle insertion) and $V_{\mathrm{N}}, b_{\mathrm{N}}, F_{\mathrm{CN}}$ are the negative (needle extraction) velocities, viscous coefficient, and Coulomb friction force respectively. F_{friction} is the friction force measured during the insertion and extraction process. The matrix form of equation (2) is shown below in equation (3),

$$\begin{bmatrix} F_{\mathrm{friction}\,1} \\ F_{\mathrm{friction}\,2} \\ \vdots \\ F_{\mathrm{friction}\,N} \end{bmatrix} = \begin{bmatrix} sgn(V_{\mathrm{P1}}) & V_{\mathrm{P1}} & sgn(V_{\mathrm{N1}}) & V_{\mathrm{N1}} \\ sgn(V_{\mathrm{P2}}) & V_{\mathrm{P2}} & sgn(V_{\mathrm{N1}}) & V_{\mathrm{N2}} \\ \vdots & \vdots & \vdots & \vdots \\ sgn(V_{\mathrm{PN}}) & V_{\mathrm{PN}} & sgn(V_{\mathrm{NN}}) & V_{\mathrm{NN}} \end{bmatrix} \times \begin{bmatrix} F_{\mathrm{CP}} \\ b_{\mathrm{P}} \\ F_{\mathrm{CN}} \\ b_{\mathrm{N}} \end{bmatrix} h. \tag{3}$$

The values of F_{CP}, b_{P}, F_{CN} and b_{N} can be calculated by using the least square method. The friction between the cannula surface and the tissue gels during the sinusoidal motion of the needle in PM tissue gels is shown in figure 6. The calculated Coulomb friction force and viscous force summing up to the total friction force at 2 mm $\mathrm{s^{-1}}$ insertion speed at different needle vibration frequencies are shown in table 1. The model could predict the friction force between 0–4 mm $\mathrm{s^{-1}}$ velocity range. However, we compared the friction at 2 mm $\mathrm{s^{-1}}$ because all experiments to measure needle insertion force, maximum needle deflection, deflection tracking error and control effort were

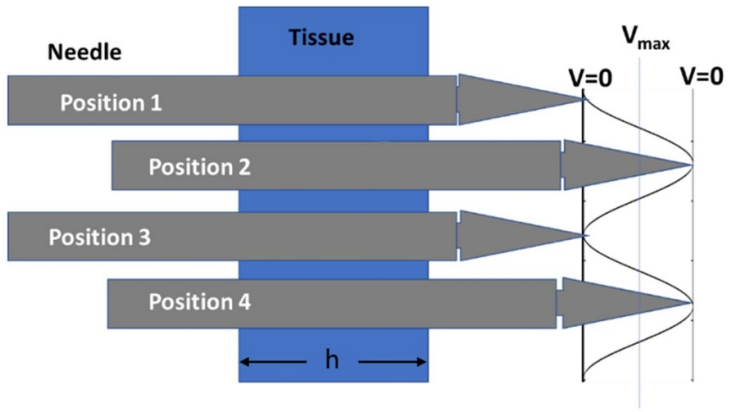

Figure 5. Schematic showing sinusoidal motion of needle shaft after passing through tissue.

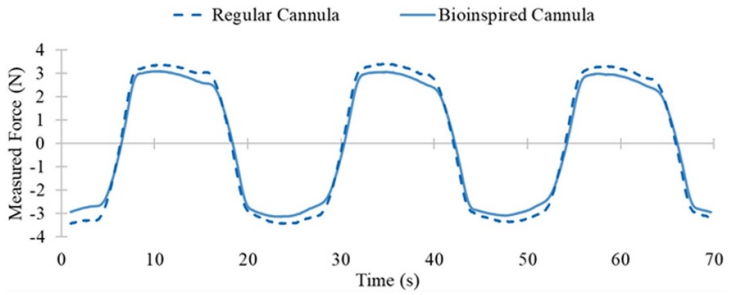

Figure 6. Force measured during sinusoidal motion of needle inside PM gel.

performed at the constant needle insertion velocity of 2 mm s^{-1}.

In this experiment, the independent variables were cannula design (regular cannula and bioinspired cannula) and frequency of needle vibration (0–400 Hz). Similarly, Coulomb force F and viscous coefficient b_P were the dependent variables. The regular cannula needle without vibration was considered a control. The bioinspired cannula design reduced the friction during insertion and extraction. Similarly, the vibrational insertion reduced the friction force for the needle with the bioinspired cannula design (see table 1). As the frequency of vibration (sinusoidal amplitude: 5 μm) was increased in the step of 100 Hz, the friction force decreased. The minimum friction force was obtained at 300 Hz frequency, after which it started to saturate. Thus, 300 Hz frequency was chosen as the vibration parameter to compare the mosquito-inspired cannula in the active needles with the regular cannula.

2.4. Measuring insertion force and tip deflection of active needles in PM gel

The effects of the mosquito-inspired cannula design and vibrational insertion method on SMA-actuated active needles were tested by measuring the insertion force and needle tip deflection during PM gel insertion. The insertion force combines cutting force at the needle tip and friction force on the needle shaft due to interaction with the tissue. The cutting force is considered constant, and friction force grows with insertion depth. Table 1 shows lower friction for bioinspired cannula design (Test 1) than regular cannula design (Test 2) when no vibration was applied. The mosquito-inspired cannula reduced the friction force and, thus, it was expected to reduce the insertion force. The decrease in friction force is due to the reduction in contact area between the needle cannula surface (maxilla structure on the needle cannula) and the tissue gel [23, 33, 34]. The active needle was first inserted up to 50 mm into the PM gel without any SMA actuation and stopped. This was followed by heating the SMA actuator to the temperature of 100 °C for full actuation, followed by additional 100 mm insertion with the fully actuated needle tip. The cannula of the PTFE tube and 3D printed polymer sheet thermally insulated the tissue gel from the 100 °C SMA wire. A proportion integral derivative controller was designed to take the temperature feedback from the SMA wire actuator with a 0.076 mm (0.003 inch) type K thermocouple (Omega, Stanford, CT) and electrically heat the SMA wire with PWM power at 0.8 Amp current to the desired temperature [29]. A six-axis force/torque transducer Nano 17® (ATI Industrial Automation, Apex, NC) was attached to the needle base and

Table 1. Total friction force measured at different needle vibration frequencies.

Test	Independent variable		Dependent variable		
	Cannula design	Vibration frequency [Hz]	Coulomb force $\left[\frac{\text{N}}{\text{m}}\right]$	Viscous coefficient $\left[\frac{\text{N s}}{\text{m}^2}\right]$	Friction at 2 mm s^{-1} $\left[\frac{\text{N}}{\text{m}}\right]$
1	Regular	0	26.55	15 645.06	57.84
2	Bioinspired	0	27.66	13 011.32	53.68
3	Bioinspired	100	27.75	12 232.43	52.22
4	Bioinspired	200	26.01	12 446.89	50.90
5	Bioinspired	300	22.77	11 635.15	46.04
6	Bioinspired	400	24.88	10 812.44	46.50

connected to a data acquisition system for measuring insertion force. The resulting needle insertion force data were obtained using LabVIEW software (National Instruments Corporation, Austin, TX). The deflection of the needle tip from 50 mm insertion depth to 150 mm depth was measured with an EM position sensor. The insertion forces and needle tip deflections of the SMA-actuated needles with two cannula designs and two insertion methods (three sample tests for each group) are presented in the results and discussion section. The statistical significance of the results was assessed using the post hoc Tukey test following analysis of variance.

2.5. Trajectory tracking control of SMA-actuated needle in PM gel

The trajectory tracking control of the active needle with the regular cannula and bioinspired cannula, with vibrational and without vibrational insertion method (three sample tests for each of the four groups) was performed inside the PM gel, and a comparison of tracking error and control effort was made. An EM position sensor was attached to the tip of the needle cannula to acquire position (x, y, z) in the 3D Cartesian coordinate space. Figure 2(e) shows the attachment of the position sensor of diameter 0.56 mm in the needle tip and its cable passing along the length of the needle. The addition of the position sensor increased the diameter of the needle by 0.11 mm. To minimize the effect of the position sensor on the needle mechanics, the needle deflection test was performed in the horizontal plane, perpendicular to the plane containing the needle axis and the position sensor. The position sensor would affect the motion of the needle, but we assumed that the effect is the same for all variations of cannula design and insertion method. The active needle was initially inserted up to 50 mm depth without actuation and stopped. The needle did not deflect because of its conical tip. Needle tip deflection tracking was performed during the needle insertion from 50 mm to 150 mm insertion depth using linear stage unislide at a constant velocity of 2 mm s^{-1}. For deflection tracking control in the PM gel, the needle tip deflection reference trajectory along the x-axis (see figure 3 for axis orientation) was created as setpoint SP_x. The position sensor measured the process variable PV_x (see equation (4)) as feedback, which was subtracted from SP_x to calculate the error e_x (see equation (5)) [6, 35]. The error e_x was fed into a PI controller programmed using LabVIEW to actuate the needle tip deflection $x(t)$ perpendicular to the insertion direction, and equal gains were used for all needle types. A generic PI controller was also used by van de Berg *et al* [35] to control the tendon-actuated needle trajectory during tissue gel insertions. The PI loop time was set to 0.1 sec such that at each loop, a new data point of the deflection trajectory was applied as a setpoint. The control effort $u_x(t)$ (see equation (6)) determined by the PI controller in LabVIEW on a duty cycle scale 0–1 was fed to the Arduino Uno on a scale of 0–255. Here, 0 means 0% duty cycle, and 255 means 100% duty cycle. The PWM digital pin of Arduino Uno supplied the signal to the metal-oxide-semiconductor field-effect transistor switch, which controlled the power in the SMA actuator. The control effort was measured by averaging the PWM duty cycle obtained on each feedback loop during the deflection trajectory tracking inside the tissue gel [29, 34]. The needle deflection tracking performance was evaluated by measuring root mean square error (RMSE) using equation (7),

$$PV_x(t) = \sqrt{(x(t) - x(0))^2} \tag{4}$$

$$e_x(t) = SP_x(t) - PV_x(t) \tag{5}$$

$$u_x(t) = K_c e_x(t) + \frac{K_c}{\tau_i} \int_0^t e_x(t)\,\mathrm{d}t \tag{6}$$

$$RMSE = \sqrt{\frac{1}{n}\sum_i (e_{xi})^2}. \tag{7}$$

3. Results and discussions

3.1. Effect of the bioinspired cannula and vibration in insertion force and needle tip deflection

The effect of the bioinspired cannula design and vibration in the active needle's insertion force into PM gel is shown in figure 7. The needle was inserted without actuation from 0 to 50 mm insertion depth followed by constant needle actuation at 100 °C SMA temperature and additional 100 mm insertion. As the insertion depth increases, friction becomes

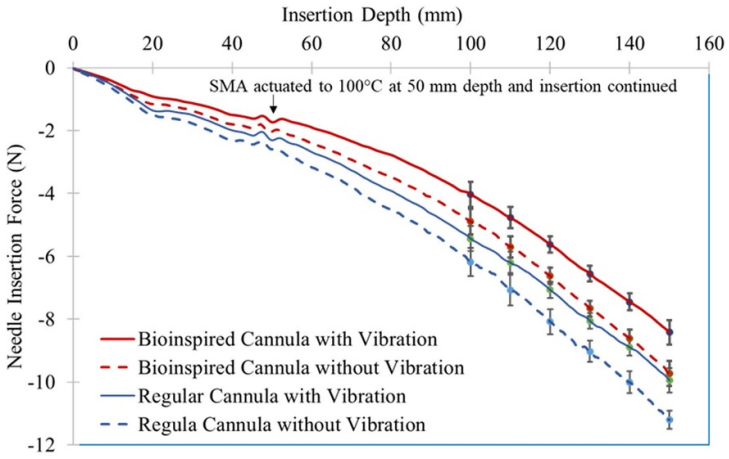

Figure 7. Insertion force in active needles for constant SMA actuation at 100 °C from 50 mm to 150 mm insertion depth.

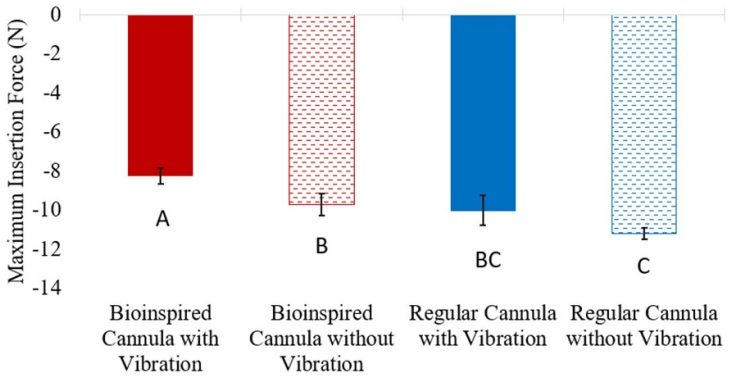

Figure 8. Insertion force at 150 mm depth for two designs of cannula and two insertion methods. Bar sharing the same letters are not significantly different at 95% level based on post hoc Tukey tests.

the main contributor to the insertion force. Figure 7 shows that the rate of change of insertion force (represented by the slopes of the curves) increased for all combinations of cannula designs and insertion methods as the insertion depth increased. This is because the actuation of active needle deflection from 50 mm to 150 mm insertion depth contributed to insertion force in addition to the needle-tissue gel friction. The mosquito-inspired cannula design and vibrational insertion mechanism reduced the insertion force throughout the insertion depth, and the reduction became significant as the insertion depth increased. The insertion force with a regular cannula was -11.20 ± 0.29 N, which was reduced to -9.73 ± 0.55 N by modifying the cannula surface with bioinspired geometry (a 13.14% reduction). The reduction of insertion force with a regular cannula by adding vibration was not significant (see figure 8). However, the combination of bioinspired shape and vibrational insertion mechanism reduced the insertion force to -8.26 ± 0.39 N (a 15.08% reduction by adding vibration and a 26.24% reduction by modifying the cannula surface profile and adding vibration). The bioinspired cannula design and vibrational insertion with the active needle in this study resulted in a decrease in insertion force like the findings of Sahlabadi and Hutapea [19] and Gidde *et al* [23] for the passive needle, despite the active needle having a larger needle tip deflection.

Figure 9 shows a picture of deflection achieved by the active needle in PM gel with the regular cannula and the bioinspired cannula design. The needle was initially inserted up to 50 mm depth without actuation (figure 9(a)), and then the SMA wire was actuated to 100 °C. After that, the needle was further inserted to 150 mm depth. Figure 9(b) shows the needle deflection with a regular cannula design, and figure 9(c) shows the needle deflection with the bioinspired cannula design at 150 mm insertion depth. The plot of active needle tip deflection inside PM gel for four combinations of cannula designs and insertion methods is shown in figure 10. The trend indicates that the bioinspired cannula design and vibrational insertion method are beneficial to achieve large tip deflection in the active needle as the insertion depth increases. Thus, adding these two bioinspired features would benefit deep tissue insertion procedures such as prostate brachytherapy [2, 3]. The needle tip

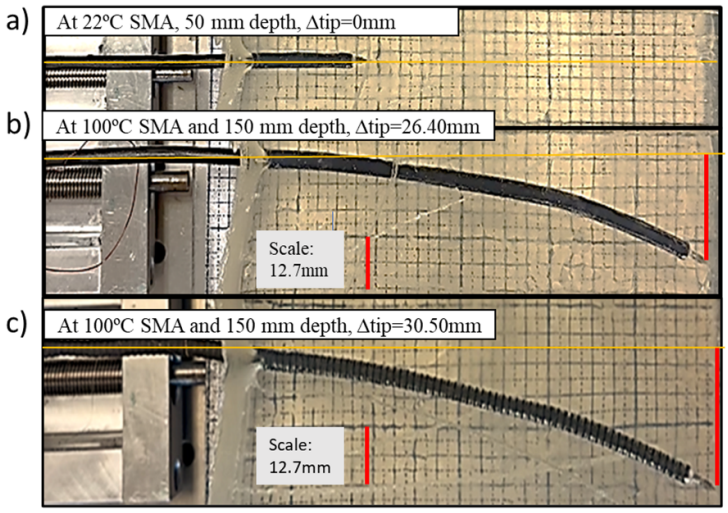

Figure 9. SMA-actuated needle insertion into PM gel: (a) initial insertion without SMA actuation, (b) needle deflection with regular cannula and SMA actuation at 150 mm insertion depth, (c) needle deflection with bioinspired cannula and SMA actuation at 150 mm insertion depth.

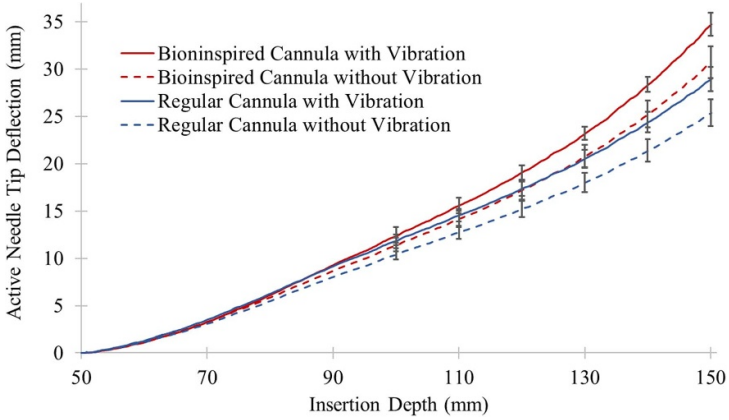

Figure 10. Tip deflection of active needles for constant SMA actuation at 100 °C from 50 mm to 150 mm insertion depth.

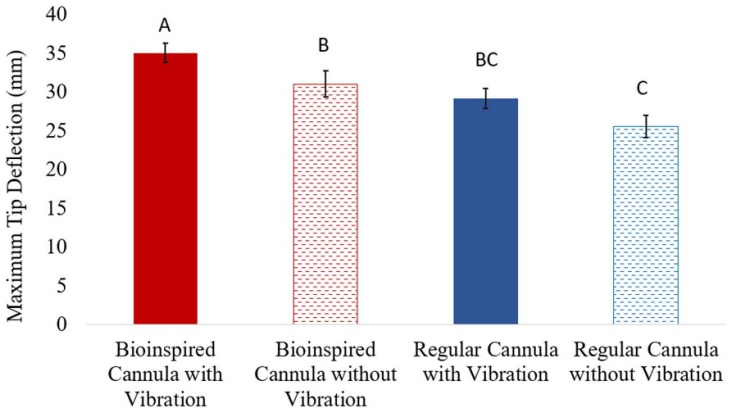

Figure 11. The active needle tip deflections at 150 mm depth for two designs of cannula and two insertion methods. Bar sharing the same letters are not significantly different at 95% level based on post hoc Tukey tests.

deflection for the regular cannula did not increase significantly by adding vibration (see figure 11). The tip deflection of the active needle at 150 mm depth with a regular cannula was 25.55 ± 1.41 mm, and by changing it with the bioinspired cannula, the deflection increased by 21.46% to 31.04 ± 1.7 mm. By adding

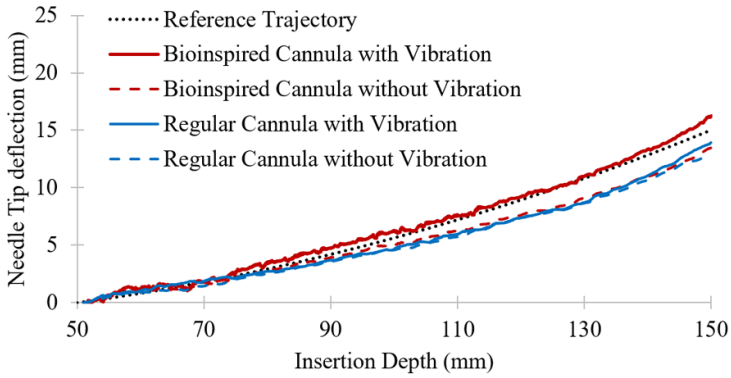

Figure 12. Deflection tracking of SMA-actuated needle inside PM gel for 100 mm depth at a velocity of 2 mm s^{-1}.

vibration to the bioinspired cannula, the active needle deflected to 35.04 ± 1.23 mm (a 12.90% increment compared to the same cannula without vibration and a 37.11% increment compared to the regular cannula without vibration).

Previous studies on passive needles with bioinspired features [19, 24] demonstrated a decrease in insertion force as well as tip deflection. The tip deflection was reduced in the passive needle because it depended solely on the interaction between the needle tip and the tissue, without any active mechanism to induce needle deflection. In contrast, the active needle in this study experienced deflection during tissue insertion due to SMA actuation. When friction is reduced due to the implementation of bioinspired features, a lower amount of SMA actuation energy is required to overcome friction, allowing a higher proportion of energy to be allocated to needle deflection. As a result, the effective bending stiffness of the active needle is reduced when friction is decreased, contributing to a greater degree of tip deflection upon SMA actuation.

3.2. Effect of the bioinspired cannula and vibration in the deflection trajectory tracking

The bioinspired cannula design and vibrational insertion method reduced the insertion force and increased the needle deflection for the same amount of SMA actuation. The reduction in the needle penetration load (represented by insertion force) during tissue gel insertion was assumed to improve the tip deflection tracking performance of the SMA-actuated needle. The results of deflection tracking control inside the PM gel with different cannula designs and insertion methods are shown in figure 12. The RMSE given by equation (7) between the actual deflection and the reference deflection trajectory during tissue insertion measures the performance of different cannula designs and insertion methods [36, 37]. Similarly, the control effort given by equation (6) shows the effort the controller puts into minimizing the deflection tracking error [38].

As the insertion depth increases, the needle cannula design and vibrational insertion method are essential in tracking the reference path. A tip deflection tracking was performed for a 100 mm needle insertion starting from 50 mm depth in PM gel to 150 mm depth. Figure 12 shows that only active needles with bioinspired features and vibrational insertion method performed well in trajectory tracking. The RMSE in deflection tracking with a regular cannula on the active needle was 1.27 ± 0.16 mm. Applying individual bioinspired features, cannula design, or vibrational insertion did not significantly improve the RMSE (see figure 13). However, using both features together, the RMSE of the bioinspired cannula design with vibration improved to 0.66 ± 0.19 mm (a 48% reduction). Figure 14 shows that the bioinspired cannula design and vibrational insertion method reduced the effort on the SMA-actuated needle for deflection tracking compared to other combinations. The control duty cycle for a regular cannula without vibration was 0.59 ± 0.02, and it improved to 0.45 ± 0.03 (a 23.25% reduction) using a bioinspired cannula and vibrational insertion. The Post hoc Tukey test shows that bioinspired cannula with vibration during deflection tracking in tissue gel achieved significantly smaller RMSE compared to (a) regular cannula with vibration (p-value = 0.0393) and (b) regular cannula without vibration (p-value = 0.0082). Similarly, the bioinspired cannula with vibration during deflection tracking in PM gel achieved a significantly smaller control duty cycle compared to (a) bioinspired cannula without vibration (p-value = 0.0003), (b) regular cannula with vibration (p-value = 0.0013), (c) regular cannula without vibration (p-value <0.0001).

3.3. Recommendations and future research

The elastic modulus of the PVC gel used in this study is close to that of prostate tissue [30]. Thus, the mechanical behavior of the needle-phantom tissue interaction is a good representation for insertion into the

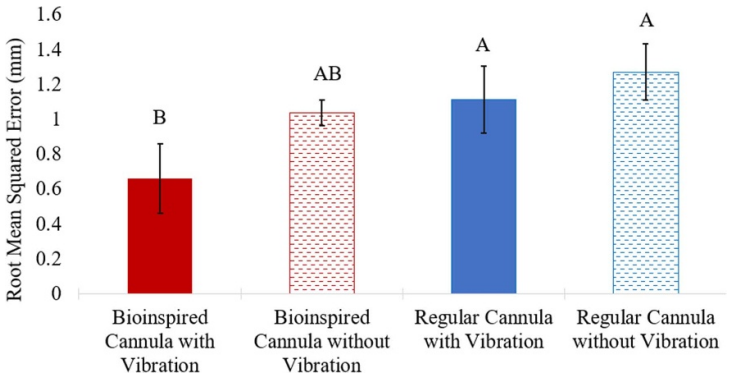

Figure 13. The root mean squared error (RMSE) in deflection tracking control of active needle for two cannulas and two insertion mechanisms. Bar sharing the same letters are not significantly different at 95% level based on post hoc Tukey tests.

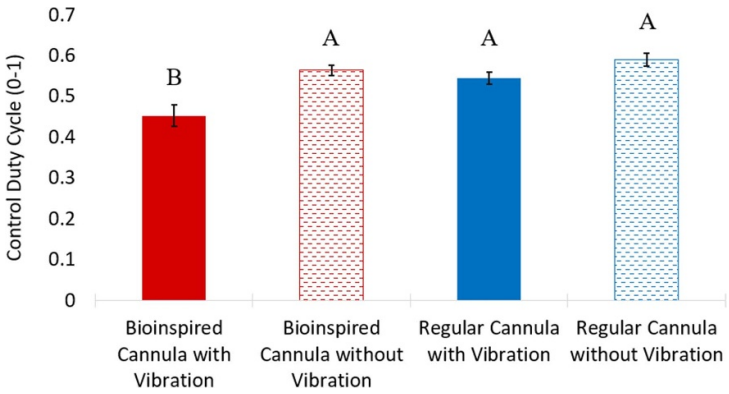

Figure 14. Control duty cycle for tracking active needle deflection for two cannulas and two insertion mechanisms. Bar sharing the same letters are not significantly different at 95% level based on post hoc Tukey tests.

prostate tissue. Since the study compares the effect of different active needles (variations in cannula geometry and insertion method), the possible error of using PVC gel instead of *ex-vivo* biological tissue can be considered insignificant [19]. However, it is recommended to perform tests on prostate tissues to see the effect due to biological tissue characteristics such as heterogeneity and viscoelasticity on the insertion path variability [39]. Furthermore, during the *in-vivo* insertion into prostate tissue, the needle passes through different tissues, such as skin and muscles, before reaching the prostate, creating a non-linear viscoelastic medium. The mechanical boundary conditions, temperature, blood flow and humidity of the prostate at *in-vivo* conditions would create changes in the needle insertion behavior that are different from *ex-vivo* insertions [40]. This study considers the initial insertion up to 50 mm depth in a straight path followed by needle deflection actuation from 50 mm to 150 mm depth to mimic the needle insertion in the *in-vivo* prostate. It was assumed that changes due to *in-vivo* conditions would similarly affect the different variations of the active needle. Nevertheless, future research should focus on performing *in-vivo* tests to prove the technical feasibility of these needles in clinical settings.

The prerequisite condition for the clinical application is the reduction of needle diameter to 14 gauge (2.11 mm diameter) and smaller. For scaling down the SMA-actuated needle, it is recommended to attach the SMA actuator to the existing needle of 1.28 mm diameter by creating a slot such that the attachment region does increase the needle diameter. This allows for using a cannula of outer diameter that could be less than 2 mm. The bioinspired cannula in this study was fabricated by 3D printing a flexible polymer sheet of 0.45 mm thickness and attaching it to the surface of the PTFE tube. It is recommended to create the mosquito-inspired maxilla structure on an existing cannula using laser cutting to reduce the outer diameter instead of adding a layer of a 3D printed sheet.

In this study, the maxilla angle and maxilla spacing optimized by Gidde *et al* [23] for a 3 mm diameter passive needle was used in the modified cannula of 3.5 mm outer diameter. The needle vibration frequency was optimized for the amplitude of 5 μm used by Gidde *et al* [23]. As the needle diameter is

scaled down, the maxilla structure dimensions, as well as needle vibration amplitude and frequency, needs to be optimized for reducing the needle-tissue interaction friction.

The position sensor attached to the needle tip impeded the needle geometry. Instead, a self-sensing mechanism such as SMA wire resistance feedback could be used for the needle deflection control [41]. In this study, needle deflection control in tissue gel was performed with a manually tuned PI controller at a low insertion speed of 2 mm s^{-1}. Advanced control strategies such as feedforward, adaptive, or model predictive control could be used to compensate for the slow response time of SMA actuation [42]. Finally, future researchers are recommended to control both the needle insertion speed as well as needle tip deflection actuation to improve the trajectory tracking for in vivo prostate insertion, where the insertion medium becomes inhomogeneous and non-linear.

4. Conclusions

This study proposed a bioinspired solution to reduce the needle tissue interaction friction and improve the active needle insertion into a PM gel. A bioinspired cannula design and vibrational insertion method inspired by the mosquito proboscis [27, 28] were applied to the SMA-actuated needle that was developed by Acharya and Hutapea [6, 29]. The data showed reduced friction with the modified features, leading to a reduction in insertion force by up to 26.24% and an increase in tip deflection by 37.11% in the SMA-actuated needle. The effect was seen more prominent as the insertion depth increased, showing the benefits for percutaneous procedures requiring deep needle penetration, such as prostate brachytherapy. The deflection tracking of the active needle during insertion into tissue-mimicking gel was also improved by adding the bioinspired features. The reduction in tracking error by 48% and control effort by 23.25% shows that the needle placement accuracy can be improved by adding the bioinspired features in the active needle.

Future work involves performing tests on PVC gel of different stiffness as well as on biological tissues to evaluate the broad applicability of the proposed bioinspired features on active needles. Similarly, optimizing the bioinspired features and using an advanced trajectory tracking controller would further enhance bioinspired active needle development.

Data availability statement

The data cannot be made publicly available upon publication because no suitable repository exists for hosting data in this field of study. The data that support the findings of this study are available upon reasonable request from the authors.

Acknowledgments

The authors would like to acknowledge the National Science Foundation (CMMI Award #1917711) for the financial support.

ORCID iDs

Sharad Raj Acharya https://orcid.org/0000-0001-7615-2041
Parsaoran Hutapea https://orcid.org/0000-0001-6917-1252

References

[1] Abolhassani N, Patel R and Moallem M 2007 Needle insertion into soft tissue: a survey *Med. Eng. Phys.* **29** 413–31
[2] Podder T K, Dicker A P, Hutapea P, Darvish K and Yu Y 2012 A novel curvilinear approach for prostate seed implantation *Med. Phys.* **39** 1887–92
[3] Li Y, Yang C, Bahl A, Persad R and Melhuish C 2022 A review on the techniques used in prostate brachytherapy *Cogn. Comput. Syst.* **4** 317–28
[4] van de Berg N J, Van Gerwen D J, Dankelman J and van den Dobbelsteen J J 2014 Design choices in needle steering—a review *IEEE/ASME Trans. Mechatronics* **20** 2172–83
[5] Acharya S R and Hutapea P 2021 Towards clinically-relevant shape memory alloy actuated active steerable needle Proc. of the ASME 2021 Conf. on Smart Materials, Adaptive Structures and Intelligent Systems *(14–15 September 2021)* p V001T05A020
[6] Acharya S R and Hutapea P 2023 Design and evaluation of shape memory alloy-actuated active needle using finite element analysis and deflection tracking control in soft tissues *Int. J. Med. Robot.* **19** e2554
[7] DiMaio S P and Salcudean S E 2005 Interactive simulation of needle insertion models *IEEE Trans. Biomed. Eng.* **52** 1167–79
[8] Abolhassani N, Patel R and Moallem M 2006 Control of soft tissue deformation during robotic needle insertion *Minim. Invasive Ther. Allied Technol.* **15** 165–76
[9] Gidde S T R, Acharya S R, Kandel S, Pleshko N and Hutapea P 2022 Assessment of tissue damage from mosquito-inspired surgical needle *Minim. Invasive Ther. Allied Technol.* **31** 1112–21
[10] Simone C and Okamura A M 2002 Modeling of needle insertion forces for robot-assisted percutaneous therapy *Proc. 2002 IEEE Int. Conf. on Robotics and Automation (Cat. No.02CH37292)* vol 2 pp 2085–91
[11] Jiang S, Li P, Yu Y, Liu J and Yang Z 2014 Experimental study of needle-tissue interaction forces: effect of needle geometries, insertion methods and tissue characteristics *J. Biomech.* **47** 3344–53
[12] Hirsch L, Gibney M, Berube J and Manocchio J 2012 Impact of a modified needle tip geometry on penetration force as well as acceptability, preference, and perceived pain in subjects with diabetes *J. Diabetes Sci. Technol.* **6** 328–35
[13] Moore J Z, McLaughlin P W and Shih A J 2012 Novel needle cutting edge geometry for end-cut biopsy *Med. Phys.* **39** 99–108
[14] Podder T, Clark D, Sherman J, Fuller D, Messing E, Rubens D, Strang J, Zhang Y, O'Dell W and Ng W 2005 Effects of tip geometry of surgical needles: an assessment of force and deflection *IFMBE Proc.* vol 11 (Citeseer) pp 1727–983
[15] Barnett A C, Lee Y-S and Moore J Z 2018 Needle geometry effect on vibration tissue cutting *Proc. Inst. Mech. Eng.* B **232** 827–37

[16] Okamura A M, Simone C and O'Leary M D 2004 Force modeling for needle insertion into soft tissue *IEEE Trans. Biomed. Eng.* **51** 1707–16
[17] Roesthuis R J, Van Veen Y R J, Jahya A and Misra S 2011 Mechanics of needle-tissue interaction *2011 IEEE/RSJ Int. Conf. on Intelligent Robots and Systems* (IEEE) pp 2557–63
[18] Patel K I, Zhu L, Ren F and Hutapea P 2021 Effect of composite coating on insertion mechanics of needle structure in soft materials *Med. Eng. Phys.* **95** 104–10
[19] Sahlabadi M and Hutapea P 2018 Novel design of honeybee-inspired needles for percutaneous procedure *Bioinsp. Biomim.* **13** 036013
[20] Chen Z, Lin Y, Lee W, Ren L, Liu B, Liang L, Wang Z and Jiang L 2018 Additive manufacturing of honeybee-inspired microneedle for easy skin insertion and difficult removal *ACS Appl. Mater. Interfaces* **10** 29338–46
[21] Li A D R, Putra K B, Chen L, Montgomery J S and Shih A 2020 Mosquito proboscis-inspired needle insertion to reduce tissue deformation and organ displacement *Sci. Rep.* **10** 12248
[22] Lenau T A, Hesselberg T, Drakidis A, Silva P and Gomes S 2017 Mosquito inspired medical needles *Proc. SPIE* **10162** 1016208
[23] Gidde S T R, Islam S, Kim A and Hutapea P 2023 Experimental study of mosquito-inspired needle to minimize insertion force and tissue deformation *Proc. Inst. Mech. Eng.* H **237** 113–23
[24] Gidde S T R, Ciuciu A, Devaravar N, Doracio R, Kianzad K and Hutapea P 2020 Effect of vibration on insertion force and deflection of bioinspired needle in tissues *Bioinsp. Biomim.* **15** 054001
[25] Scali M, Kreeft D, Breedveld P and Dodou D 2017 Design and evaluation of a wasp-inspired steerable needle *Proc. SPIE* **10162** 1016207
[26] Izumi H, Yajima T, Aoyagi S, Tagawa N, Arai Y, Hirata M and Yorifuji S 2008 Combined harpoonlike jagged microneedles imitating mosquito's proboscis and its insertion experiment with vibration *IEEJ Trans. Electr. Electron. Eng.* **3** 425–31
[27] Izumi H, Suzuki M, Aoyagi S and Kanzaki T 2011 Realistic imitation of mosquito's proboscis: electrochemically etched sharp and jagged needles and their cooperative inserting motion *Sens. Actuators* A **165** 115–23
[28] Kong X Q and Wu C W 2009 Measurement and prediction of insertion force for the mosquito fascicle penetrating into human skin *J. Bionics Eng.* **6** 143–52
[29] Acharya S R and Hutapea P 2022 Design and control strategy of tip manipulation for shape memory alloy actuated steerable needle Proc. of the ASME 2022 Conf. on Smart Materials, Adaptive Structures and Intelligent Systems (*Dearborn, Michigan, 12–14 September 2022)* p V001T04A011
[30] Ahn B-M, Kim J, Ian L, Rha K-H and Kim H-J 2010 Mechanical property characterization of prostate cancer using a minimally motorized indenter in an ex vivo indentation experiment *Urology* **76** 1007–11
[31] Li W, Belmont B and Shih A 2015 Design and manufacture of polyvinyl chloride (PVC) tissue mimicking material for needle insertion *Proc. Manuf.* **1** 866–78
[32] Richard C, Cutkosky M R and MacLean K 1999 Friction identification for haptic display *ASME Int. Mechanical Engineering Congress and Exposition* vol 16349 (American Society of Mechanical Engineers) pp 327–34
[33] Acharya S R, Kim D and Hutapea P 2023 Mosquito-inspired cannula to improve control of active surgical needle in soft tissue *Int. Mechanical Engineering Congress & Exposition* (American Society of Mechanical Engineers (ASME))
[34] Acharya S R, Kim D and Hutapea P 2023 Steering control improvement of active surgical needle using mosquito-inspired cannula *J. Eng. Sci. Med. Diagn. Ther.* **6** 041101
[35] van de Berg N J, Dankelman J and van den Dobbelsteen J J 2015 Design of an actively controlled steerable needle with tendon actuation and FBG-based shape sensing *Med. Eng. Phys.* **37** 617–22
[36] Deaton N J, Brumfiel T A, Sheft M, Yamamoto K K, Elliott D, Patel P and Desai J P 2023 Towards steering a high-dose rate brachytherapy needle with a robotic steerable stylet *IEEE Trans. Med. Robot. Bionics* **5** 54–65
[37] Joseph F O M and Podder T 2018 Sliding mode control of a shape memory alloy actuated active flexible needle *Robotica* **36** 1188–205
[38] Villoslada Á, Escudero N, Martín F, Flores A, Rivera C, Collado M and Moreno L 2015 Position control of a shape memory alloy actuator using a four-term bilinear PID controller *Sens. Actuators* A **236** 257–72
[39] Majewicz A, Wedlick T R, Reed K B and Okamura A M 2010 Evaluation of robotic needle steering in ex vivo tissue *2010 IEEE Int. Conf. on Robotics and Automation* (IEEE) pp 2068–73
[40] Podder T, Clark D, Sherman J, Fuller D, Messing E, Rubens D, Strang J, Brasacchio R, Liao L and Ng W 2006 In vivo motion and force measurement of surgical needle intervention during prostate brachytherapy *Med. Phys.* **33** 2915–22
[41] Berhil A, Barati M, Bernard Y and Daniel L 2023 Accurate sensorless displacement control based on the electrical resistance of the shape memory actuator *J. Intell. Mater. Syst. Struct.* **34** 1097–103
[42] Hoseini S F, MirMohammadSadeghi S A, Fathi A and Daniali H M 2021 Adaptive predictive control of a novel shape memory alloy rod actuator *Proc. Inst. Mech. Eng.* I **235** 291–301